Korean J. Chem. Eng., 33(5), 1620-1628 (2016)
DOI: 10.1007/s11814-015-0292-7

pISSN: 0256-1115
eISSN: 1975-7220

Phenol decomposition in water cathode of DC atmospheric pressure discharge in air

Elena S. Bobkova*, Dmitriy S. Krasnov, Alexandra V. Sungurova*, Vladimir V. Rybkin**,†, and Ho-Suk Choi***,†**

*Department of Industrial Ecology, Ivanovo State University of Chemical Technology, Ivanovo 153000, F. Engels 7, Russia
**Department of Electronic Devices and Materials, Ivanovo State University of Chemical Technology, Ivanovo 153000, F. Engels 7, Russia
***Department of Chemical Engineering, Chungnam National University, 220 Gung-dong, Yuseong-gu, Daejeon 34134, Korea
(*Received 19 June 2015 • accepted 19 December 2015*)

Abstract−We studied phenol decomposition in aqueous solution under the action of DC discharge at atmospheric pressure in air. The decomposition efficiency was 0.017 molecules per 100 eV. When the kinetics of forming destruction products was studied in detail, the peculiarities of air plasma action were revealed for the first time. Plasma action not only results in the formation of oxygen-containing products, which are usually formed under oxygen plasma action (hydroxyhenols, carboxylic acids, aldehydes), but also the formation of nitro phenols. The treatment is accompanied by hydrogen peroxide formation, a pH decrease, and nitric and nitrous acids formation. We also discussed the possible mechanism of the processes and the role of some active species in chemical transformations after determining some parameters of the discharge.

Keywords: Phenol, Decomposition, Kinetics, Discharge, Decomposition Products, Air

INTRODUCTION

Finding solutions to the problems encountered converting organic waste in the water purification process is of great research importance. The conventional methods based on chlorination or ozonation are rather expensive and often ineffective. A promising technique is the application of various types of gaseous discharges, the so-called advanced oxidation technologies (AOT). To date, many devices have been tested for this purpose (e.g., corona discharge over solution surface [1], contact glow discharge electrolysis [2,3], pulsed streamer discharge in or above solution [4,5], dielectric barrier discharge [6,7] and gliding arc [8]). At the same time, the data on DC discharge at atmospheric pressure with a liquid cathode are rather limited in spite of the fact that such discharge is the simplest for technical realization. In a study [9], it was shown that this discharge was effective in the discoloration process of a water solution of potassium permanganate and potassium cyanate. The discharge action resulted in the discoloration of the water solution due to some organic dyes and the oxidation of the I^- ions [10]. The discharge decomposition of organics in aqueous solution has also been reported in recent articles [11,12].

This study proposes a decomposition mechanism in that type of discharge and compares the discharge efficiency with other types of discharges. An aqueous phenol solution was chosen for testing due to the following reasons. First, phenol is classified as a teratogenic and carcinogenic agent. Its biodegradability is only 90% in surface waters after seven days. Second, the compound is among the most studied and thus it is possible to make an appropriate comparison. Although the destruction of phenol was studied in detail for various types of discharges [1-5], the data on kinetics and composition of destruction products are rather limited. There are some fragmentary data on separate products, but the detailed studies of product kinetics are not available. Recent studies have reported the effective rate constants of phenol decomposition for DC discharge in air and also revealed that the phenol decomposition results in the formation of aldehydes and carboxylic acids [13, 14]. Our calculation of product balance, however, expects that other compounds have to be formed as well. Thus, complete data are necessary to reveal the process mechanism and estimate the quality of water purification. It is also clear that ambient air is the most preferable plasma forming gas from the viewpoint of process economics. It is necessary to underline that specific features of air application in comparison with oxygen have not been studied yet, except for the data which shows that oxygen is more effective than air for phenol removal [1,15].

EXPERIMENTAL

1. Experimental Setup

Fig. 1 shows the scheme of the setup used in our work. The discharge cell was open to ambient air, so there was no gas control. DC power supply was used for the excitation of discharge under atmospheric pressure (AP). High voltage (up to 4 kV) was applied between the liquid cathode and copper anode placed at the position of 3 mm above the solution surface. The anode was a copper wire 2 mm in diameter, which was sharpened to a point. The phe-

†To whom correspondence should be addressed.
E-mail: rybkin@isuct.ru, hchoi@cnu.ac.kr

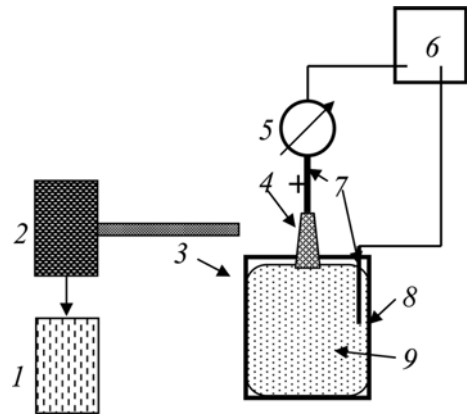

Fig. 1. The schematic diagram of the experimental setup.

1. Data acquisition system
2. Monochromator
3. Light guide
4. Plasma flame
5. Ampere meter
6. Direct current power supply
7. Electrodes
8. Reaction vessel
9. Solution

nol solution was connected to the negative pole of power supply with the aid of a 9 cm diameter copper ring electrode made from the same wire. The distance between the anode and liquid surface was adjustable. The discharge current was 40 mA. The solution volume was 80 ml and the solution depth was 1 cm. An aqueous phenol solution of 50 mg/*l* concentration was used. We observed the evaporation of the solution during discharge process. Within the time of experiment, however, the lowering in solution level was negligible. It was experimentally checked through emission spectrum as well.

2. Measurements

2-1. Discharge Analysis

The discharge voltage between the anode and negative electrode was measured as a function of the distance between the anode and liquid surface. The voltage drop on the water layer was measured at the point of anode contact with the solution surface. This value was then subtracted from the voltage being measured. The voltage-distance dependence was extrapolated to a distance of zero to obtain the cathode drop value and electric field strength (E) in the plasma column. The emission spectra were recorded within the wavelength range of 200-900 nm using a compact multipurpose two channel Avaspec-2048 monochromator with the grating of 600 line/mm and the resolution of 0.34 nm. The spectral sensitivity of the optical system was calibrated.

2-2. Chemical Analysis

After a fixed time of discharge action, the solution samples were chemically analyzed. The concentrations of phenol and aldehydes were measured using the fluorescent method (Spectrofluorimeter Fluorat - 02, Russia). The phenol was extracted into butyl acetate, then re-extracted into a water solution followed by acidation. The photometric method was used to determine total concentration of hydroxyderivatives of phenol (catechol, resorcinol and hydroquinone) by means of their reaction with 4-aminoantipyrine (4-amino-2,3-dimethyl-1-phenyl-3-pyrazolin-5-one) in the presence of potassium hexacyanoferrate ($K_3[Fe(CN)_6]$) in an alkaline medium (pH=10) followed by absorbance measurement at the wavelength, λ, of 540 nm. In the case of aldehydes, a fluorescent substance was formed as a product of the reaction between aldehydes and 1,3-cycloxehanedione in the presence of ammonium ions. The concentration of hydrogen peroxide was determined by titration, which was based on the oxidation of I^- ion by peroxide followed by the reduction of iodine with sodium thiosulfate with the use of a starch solution as an indicator for iodine. Additionally, several points were checked with the colorimetric method using the reaction of H_2O_2 with titanyl ions by the analysis of the maximum absorbance of the peroxotitanium (IV) complex at the wavelength of 410 nm [16]. The difference was less than 10%. Thus, the concentrations of other components that are able to oxidize I^- ions (for example, ozone, peroxynitrous acid etc.) have to be essentially less than the hydrogen peroxide concentration.

2-3. Absorbance Analysis

The total concentration of carboxylic acids was obtained by measuring the absorbance of the color reaction of acids with m-ammonium vanadate at the wavelength of 400 nm. Since hydrogen peroxide forms with vanadate (the colored compound absorbed on the same wavelength), the absorbance of the latter was measured using a specially prepared reference solution and the appropriate absorbance value was taken into account. The concentration of nitrate ions was measured using color reactions with salicylic acid (λ=480 nm). The method of nitrite determination was based on diazotization of sulfanilic acid and on the formation of red-violet dye of the diazo compound with α-naphthyl amine followed by the absorbance measurements at the wavelength of 520 nm. The oxidizers (for example, peroxy nitrous acid) presenting in the solution are able to react with the dye resulting in discoloration. But we did not observe any significant absorbance changes during the first 8 minutes after preparing the solution. All reagents were analytical grade (Sigma Aldrich).

A Hitachi U-2001 spectrophotometer was used for measuring the absorption spectra. For every analysis, a fresh portion of the solution was used. The reproducibility of measurements was checked using the results of five measurements, and a confidence coefficient of 0.95 was applied in the calculation of errors.

RESULTS AND DISCUSSION

1. Analysis of Discharge and Emission Spectrum

The measurements have shown that the total voltage drop on discharge was 863 V, cathode voltage drop was 558 V and electric field strength in plasma was 900 V/cm under the given conditions. The cathode voltage drop is shown in Fig. 2. Another part of an applied voltage was dropped on the ballast resistance (30 kΩm).

The gas temperature measurement was based on analysis of the unresolved rotational structure for the electronic-vibrational bands of nitrogen. The most intensive bands in emission spectrum are the bands of the N_2 second positive system($C^3\Pi_u \rightarrow B^3\Pi_g$ transition). The OH band ($A^2\Sigma \rightarrow X^2\Pi$ 0-0) normally used for the temperature measurements [17] is also presented, but the use of this band is not convenient. First, the OH band intensity is noticeably lower than the intensity of the N_2 bands. Second, the OH band is partially overlapped by the nitrogen bands. From the last point of

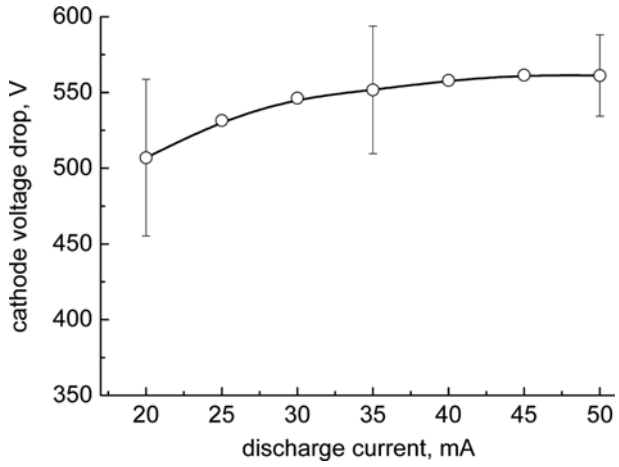

Fig. 2. The cathode voltage drop as a function of discharge current.

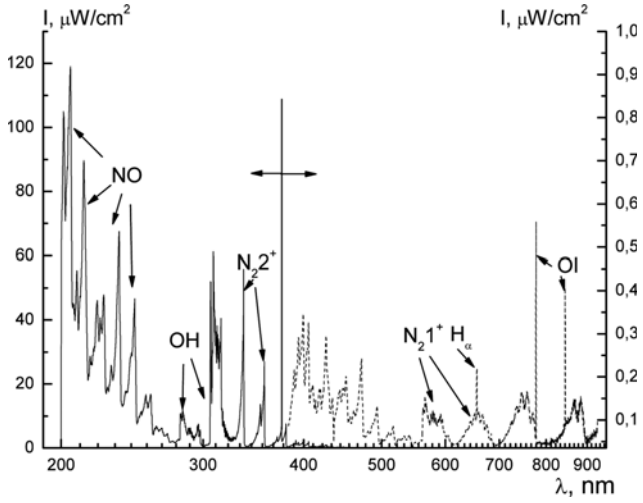

Fig. 3. Emission spectrum of discharge. μW/cm² means power per unit area of the entrance slit of the monochromator.

view, the $C^3\Pi_u \rightarrow B^3\Pi_g$, 0-2 band looks more attractive. This band is clearly observed in emission spectrum (Fig. 3, 381 nm).

The appropriate analysis of the rotational structure allows us to obtain the "rotational" temperature of definitely excited state only. To identify this temperature with translational temperature, the condition $\tau_{rot} >> \tau_r$ (τ_{rot}-characteristic time of rotational relaxation, τ_r-radiation lifetime) has to be valid. For the $C^3\Pi_u$, V=0 states the τ_r is about 4.45×10^{-8} s. The τ_{rot} can be estimated as

$$\tau_{rot} = \left(\frac{V\times\sigma\times N}{Z}\right)^{-1} = \left(\sqrt{\frac{8\times k\times T}{\pi\times m}}\times\frac{\sigma}{Z}\times\frac{P}{k\times T}\right)$$

where V is the velocity of relative movement, σ is the gas-kinetic cross section for the colliding molecules, N is the density of particles, Z is the average amount of gas-kinetic collisions resulting in rotational relaxation, m is a reduced mass, P the pressure, T the gas temperature, k is the Boltzmann constant. For the N_2 molecule, the gas kinetic diameter is 3.5×10^{-8} m and Z≈6. Taking T=2000 K and P=1×10^5 Pa for the estimation, we obtain $\tau_{rot}\approx1.6\times10^{-12}$ s. Therefore, the "rotational" temperatures are very close to the translation temperatures.

Assuming the Boltzmann distribution of molecules on rotational levels, the irradiation intensity of rotational line, I, can be expressed as

$$I(J', J'') = const\times\nu^4(J', J'')\times S(J', J'')\times\exp\left[-\frac{hc\times F(J')}{k\times T}\right]$$

where J′ and J″ are the rotational quantum numbers for upper and lower levels, respectively, ν(J′, J″) the transition frequency, S(J′, J″) is the intensity factor, c is the light velocity, h is the Planck constant, F(J′) is the rotational term of upper state and "const" is a constant for the definite transition. Unresolved structure of band is formed as an overlapping of separate line profiles, which are determined by the monochromator transfer function. According to reference [18], the $C^3\Pi_u \rightarrow B^3\Pi_g$, 0-2 band consists of R_1, R_2, R_3, P_1, P_2, P_3, Q_2, and Q_3 branches.

The spectrometer transfer function was obtained by means of profile measurement of single Ar-lines using the Ar-low pressure lamp as a source. The relative band profile was calculated using the gas temperature as a parameter. This profile was normalized to the peak band intensity and fitted through the least square method. Fig. 4 shows an example. The accuracy of temperature obtained by this way was about ±100 K. These errors are less than reproducibility errors. The reproducibility errors were calculated on the basis of five and more measurements using the confidence probability of 0.9. The possibility of applying this method was additionally checked. The MDR23 spectrometer was utilized. Its grating of 1200 line/mm allows us to obtain the resolved structure of R_1-branch (for J′>15) and unresolved one depending on the split sizes. The temperatures obtained were the same within the range of ±25 K.

The gas temperature, obtained by modeling the non-resolved structure of the N_2 band $C^3\Pi_u \rightarrow B^3\Pi_g$ (0-0) as it was described in our previous study [19], was 1,900±100 K. Thus, the reduced electric field strength E/N was 23 Td and the total power input into the discharge was 34.5 W. The initial solution conductivity was 36 μS/cm and final (after 60 min) was 120 μS/cm.

An overview of the emission spectrum is shown in Fig. 3. The

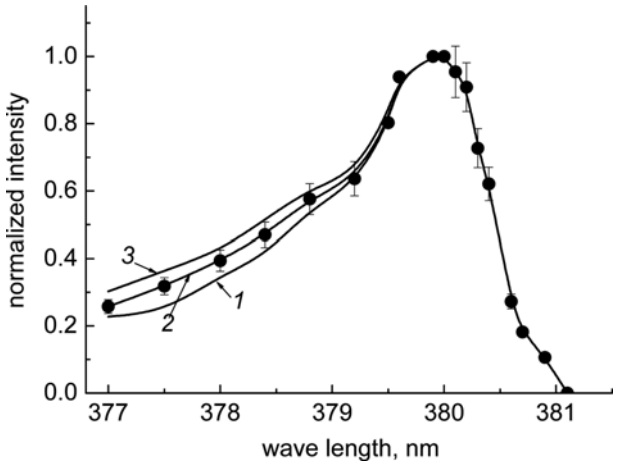

Fig. 4. Calculated (1-3) and experimental (2) profiles of the $C^3\Pi_u \rightarrow B^3\Pi_g$, 0-2 band. 1, 2, 3 - gas temperature of 1,700, 1,900, and 2,100 K, respectively.

spectrum was corrected for the wavelength-dependent sensitivity of the spectrometer. The following lines and bands were presented. Molecular nitrogen: The most intense signals were the second positive system bands (N_2 2^+). They were represented by (1-2); (0-1); (2-4); (1-3); (0-2); (3-6); (2-5); (1-4); (0-3); (4-8), (3-7); and (2-6) overlapped bands. The bands of the first positives ($B^3\Pi_g \rightarrow A^3\Sigma_u^+$, N_2 1^+) were present as well.

Atomic oxygen (OI): There were 777 nm ($3p^5P \rightarrow 3s^5S$) and 845 nm ($3p^3P \rightarrow 3s^3S$) lines.

The radiation bands of OH-radicals and nitric oxide (NO) were the main bands in the UV region. For OH, there were two bands: $A^2\Sigma \rightarrow X^2\Pi$ (1-0) and $A^2\Sigma \rightarrow X^2\Pi$ (0-0). The NO spectrum was represented by a set of overlapped bands of the γ-system ($A^2\Sigma \rightarrow X^2\Pi$) corresponding to (1-0), (2-2), (0-0), (0-1), (0-2), (0-3) and (0-4) transitions between various vibration states.

Irradiation of atomic hydrogen was represented by H_α (656 nm). Note that the bands of carbon monoxide as a product of organic decomposition were not observed in the limit of sensitivity.

2. Kinetics of Phenol Decomposition

The phenol decomposition kinetics is shown in Fig. 5. The data were obtained by using the fluorescent method and absorption method at the wavelength of 260 nm (see also Fig. 9). The results have shown that phenol decomposition is accompanied by the formation of the products absorbing in the same wave range. Therefore, the application of an absorption method, which is rather frequently used, is not appropriate under these conditions. Unlike an impulse corona [4] and glow discharge electrolysis [2,3], the phenol decomposition kinetics do not obey the first order kinetics. By increasing phenol concentration at fixed discharge parameters, the kinetic law can be changed from first to zero order in a solute. Such behavior can be explained by the limitation of phenol decomposition due to the formation rate of active species, which react with phenol. In this case, the decomposition rate is equal to the formation rate of active particles, which means that the rate does not depend on the phenol concentration and the kinetic law becomes zero order. This conclusion confirms the review [20].

Therefore, for a correct comparison, it is necessary to provide the same phenol concentration and the composition of active species, which react with phenol. It is clear that the latter condition is very difficult to fulfill. Most likely, this is the reason why the data obtained by various authors significantly differ. Thus, the maximum rate constants are located in the range of $(0.6\text{-}6)\times10^{-4}$ s^{-1} [2-4]. The approximation of an initial part of the kinetic curve with the first-order law gives the rate constant of 7×10^{-3} s^{-1}. The closest results that can be compared to ours were obtained in a previous study [4] in which the same phenol concentration (47 mg/*l*) was used. But the impulse corona (above) was discharged into a mixture of oxygen and argon. The maximum energetic yield of phenol decomposition was obtained for the discharge in oxygen over the solution. It was equal to 0.0132 molecules per 100 eV at the phenol decomposition degree of 0.63. In the case of underwater discharge, the appropriate value was 0.0019. The value calculated from our data was 0.017 molecules per 100 eV. The energetic yield, α, of phenol decomposition was calculated by using the following equation:

$$\alpha = \frac{0.63 \times C_0 \times V \times 1.6 \times 10^{-19} \times 100 \times K}{W},$$

where C_0 is the initial phenol concentration (cm^{-3}), V is the solution volume (cm^3), K is the effective rate constant of phenol decomposition (s^{-1}), W is the discharge power (W), 1.6×10^{-19} is the electron charge.

The value of ~2 (decomposition degree of 0.4) was obtained for pulsed positive corona discharge in oxygen over the solution in previous study [1] and the value of 0.025 (decomposition degree of 0.4) for DBD discharge in dry air [21]. The value of 0.0106 was obtained for pulsed corona in water solution of phenol (0.27 mmol/*l*) in previous study [22]. It is possible to improve the energetic yield of discharge under study by applying the higher discharge current or using multiple anode needles in a gas phase. This allows the area of the discharge-solution contact surface to increase. In the given case, the diameter of the cathode spot was only 4 mm.

3. Formation and Kinetics of By-products

3-1. Formation and Kinetics of Oxygen-containing Products

Most studies assume that the primary reactions leading to the destruction are reactions of phenol with •OH hydroxyl radicals. This assumption is based upon the composition of by-products, the influence of adding Fenton's reagent and radical scavengers, and the decomposition rate. The formation of hydroxyderivatives of phenol (hydroquinone, resorcin, pyrocatechol) is a result of •OH attachment to phenol as follows.

$$C_6H_5OH + \bullet OH \rightarrow H_2O + \bullet C_6H_4OH, \quad \bullet C_6H_4OH + \bullet OH \rightarrow C_6H_4(OH)_2$$

The above reactions were confirmed in previous studies [2,4,5]. In our case, the oxyphenols are formed as well. The kinetics of their formation is presented in Fig. 6. The kinetic curve shape clearly shows that the oxyphenols are intermediate products.

The addition of Fe^{2+} salts to the solution resulted in the increase in phenol decomposition rates [2,3,22-24] due to $Fe^{2+} + H_2O_2 \rightarrow Fe^{3+} + OH^- + \bullet OH$ reaction. As a result of this reaction, recent studies observed a decrease in the hydrogen peroxide concentration [25, 26]. The addition of t-butanol, which is a scavenger of •OH-radicals, resulted in the decrease in the phenol decomposition degree

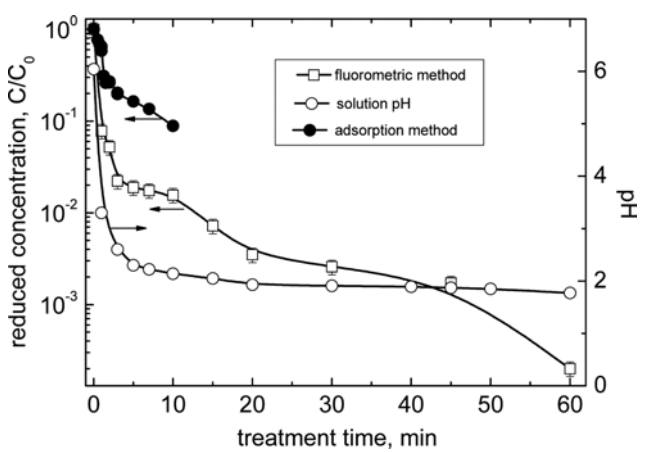

Fig. 5. The variation of phenol concentration and solution pH during plasma treatment. C_0=50 mg/*l*. Phenol concentration was determined by both fluorescent and adsorption methods.

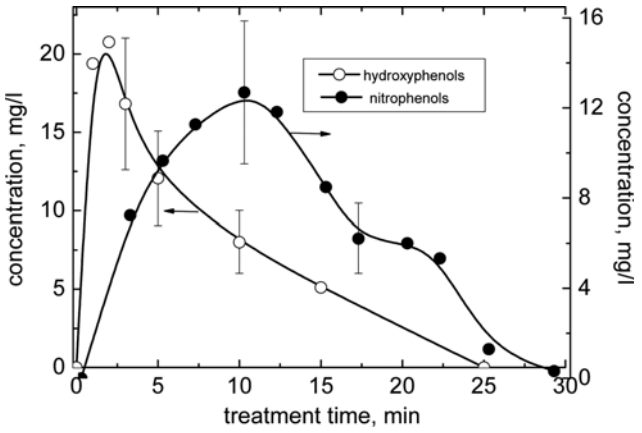

Fig. 6. The variation of hydroxyphenol and nitrophenol concentrations during plasma treatment.

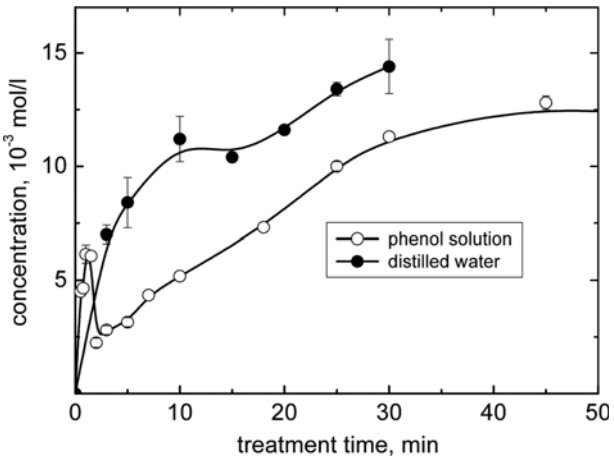

Fig. 7. The variation of hydrogen peroxide concentration in distilled water and phenol solution during plasma treatment.

[1]. At the same time, the addition of alcohols (ethanol and 2-propanol) in the optimal amount (up to 0.1 mol/*l*) increased the hydrogen peroxide concentrations in glow discharge over water [27]. That fact can be explained as follows: •OH-radicals participate both in the reactions of H_2O_2 formation via $\bullet OH+\bullet OH\rightarrow H_2O_2$, $K=5.5\times10^{10}$ *l*/(mol×s) and simultaneously react with the hydrogen peroxide via $H_2O_2+\bullet OH\rightarrow HO_2\bullet+H_2O$, $K=2.7\times10^{7}$ *l*/(mol×s) reaction. The ratio between the rates of these reactions will define the behavior of H_2O_2 concentration. •OH radicals can be formed as a result of the dissolution of hydrogen peroxide formed in a gas phase followed by H_2O_2 dissociation. Particularly, the pathway was used in previous study [28] for the explanation of H_2O_2 formation in the oxygen bubble DBD. The radiation spectrum (Fig. 3) clearly shows the formation of •OH radicals in a gas phase. These radicals can dissolve in water as well. Henry's constant is $25\times\exp[5280(1/T-1/298)]$ $mol^{-1}L^{-1}atm^{-1}$ [28]. Nevertheless, the OH lifetime is short in a gas phase; the •OH concentration measured in DC discharge by the laser-induced fluorescence (LIF) method at the current of 30 mA was $N_{OH}\approx2\times10^{16}$ cm^{-3} [29]. •OH flux (J_{OH}) onto a solution surface can be estimated as $J_{OH}=(1/4)N_{OH}\times\overline{V}=(1/4)N_{OH}\times\sqrt{8kT/\pi M}$ (*k*-Boltzmann constant, T (=1900 K)-gas temperature, *M*-mass of OH molecule). If all •OH radicals react in a liquid, the possible process rate is $W=J_{OH}\times(S_S/V_S)$ (S_s-cathode spot square, V_S-solution volume). The calculation gives the W value of 4.4×10^{17} $cm^{-3}c^{-1}$; the phenol decomposition rate as $t\rightarrow0$ is 2.2×10^{15} $cm^{-3}c^{-1}$ (Fig. 5), and the hydrogen peroxide formation rate for the phenol solution as $t\rightarrow0$ is 9×10^{16} $cm^{-3}c^{-1}$ (Fig. 7). Therefore, •OH radicals forming in a gas phase are able to provide the observed rates of processes. The other method of •OH formation is non-equilibrium dissociation of water molecules under the impact of ions accelerated in a cathode voltage drop, which is $H_2O+ion\rightarrow\bullet H+\bullet OH+ion$. The value of a cathode drop (558 V) is enough for water dissociation. The temporal dependence of hydrogen peroxide concentration is shown in Fig. 7. The results for distilled water are given as well. When the phenol concentration is quite large, the phenol induces the formation of H_2O_2 in the initial step of the discharge action, which means that there are at least two independent pathways of H_2O_2 formation. One of them is connected with the reaction of •OH dimerization. And the other may be the reaction of excited states of water molecules $2H_2O^*\rightarrow H_2+H_2O_2$, which was proposed in the previous study [5] when modeling the processes of phenol decomposition in pulsed streamer corona. Most likely, after the phenol has been exhausted, the products of its decomposition continue to react with the •OH radicals but the rate constants will change.

Certainly, ozone can react with phenol as well. But there are no direct measurements of ozone contribution in a decomposition process. Thus, the addition of t-butanol of 0.5-2 mM concentration into 1 mM solution of phenol resulted in the decrease in phenol decomposition efficiency from 45% to 40% [1], and the same values of 40% were obtained for 1 and 2 mM concentrations of t-butanol. The authors assume that all •OH radicals reacted with t-butanol and 40% efficiency is provided with ozone, whereas 5% is provided with •OH. This result is rather unusual since phenol is a stronger •OH scavenger than t-butanol. The rate constant of the reaction between phenol and •OH is 6×10^{10} *l*/(mol×s) [30], whereas the rate constant is only 6.5×10^{8} *l*/(mol×s) for t-butanol [31]. According to these constants, the addition of t-butanol at the concentrations mentioned above has no effect on the •OH concentration. The ozone contribution to phenol decomposition was estimated to be 30% in another study using DBD [16]. The addition of ozone (concentration is unknown) to an underwater pulsed corona resulted in the increase in energetic yield of phenol decomposition from 0.0106 to 0.041 molecules/100 eV [22]. The molecular phenol decomposition rate in positive pulsed corona under Ar atmosphere was sensibly higher than that under O_2 atmosphere, and the compositions of decomposition products were similar [4]. The rate constant of reaction between ozone and phenol in acid media is 1.3×10^{3} *l*/(mol×s) [4], which is 10^{7} times less than that of •OH. To provide the essential ozone contribution, its concentration has to be more than that of •OH by 10^{7} times. We tried to measure ozone concentration on the absorption at the wavelength of 254 nm (Hg-lamp). But we could not detect any absorption peaks. On the basis of the system parameters, the upper limit of ozone concentration in a gas phase was estimated as 85 μmol/*l*. Modeling chemical composition carried out in a study [32] gave the value of ~4×10^{-4} f μmol/*l* for the same discharge conditions. In a solution,

the concentration has to be less. In a study [33] devoted to modeling the chemical process kinetics in our discharge type under the same conditions, •OH concentration was in the range of (0.01-0.001) μmol/*l*. The comparison of these data shows that the direct ozone contribution cannot be too high. Ozone is able to have an influence on the process of organic decomposition in an indirect way over the reactions of formation and destruction of •OH radicals.

•OH formation proceeds via reaction [34]:

$$O_3+HO_2^-\rightarrow \bullet OH+O_2^-+O_2 \qquad (K=2.2\times10^6\ l/(mol\times s))$$

But the acidic form of hydrogen peroxide reacts with ozone extremely slowly due to a low concentration of HO_2^- ions [35]. Ozone can remove •OH radicals via reaction [36];

$$O_3+\bullet OH\rightarrow HO_2+O_2 \qquad (K=2\times10^9\ l/(mol\times s))$$

The •OH lifetime for the process of its reaction with phenol is $(K\times[Ph]^{-1}=3.1\times10^{-8}$ s (K is the rate constant equal to 6×10^{10} *l*/(mol×s), [Ph]=0.53 mmol/*l* is phenol concentration). The •OH lifetime for the process of its reaction with ozone is $(K\times[O_3]^{-1}=6.3\times10^{-4}$ s (K is the rate constant equal to 2×10^9 *l*/(mol×s, $[O_3]$=85 μmol/*l* is the estimated ozone concentration). The comparison of these values shows that the indirect ozone action is not essential.

3-2. Formation and Kinetics of Nitrogen-containing Products

For air plasma, it is also possible to form peroxynitrous acid via $NO+HO_2\bullet\rightarrow ONOOH$ reaction ($K=3.2\times10^7$ *l*/(mol×s)) in a liquid phase [37]. That compound has a rather strong oxidative action. The standard oxidation E^0 (V/SHE) of the $ONOOH/NO_2$ reported in a study [37] was about 1 V lower than that of OH/H_2O and is a stronger oxidizer than H_2O_2/H_2O. But, so far as we know, any experimental data on this problem are not available.

The change of solution temperature during the treatment was measured (Fig. 8). The temperature rapidly rises and tends to plateau for 6 min. The temperature increase clearly affects the process kinetics but not too strongly since the reactions of radicals have, as a rule, low activation energy. Thus, the activation energy of reaction between phenol and •OH is 7.7 kJ/mol [38].

Fig. 9 shows the changes in the UV absorption spectrum of solution. On starting the discharge action, the solution gradually turned yellow, implying the occurrence of destruction products. After 20 min of treatment, the color disappeared. The color change reported in the other study [3] was attributed to the formation of oxyphenols such as p-benzoquinone, hydroquinone and catechol. But that attribution is not correct since the water solution of these compounds is colorless because the absorption is in the range of short-wave ultraviolet light. As an example, Fig. 10 shows the absorption spectrum of catechol, which is the main product among other hydroxyphenols according to the other study [4].

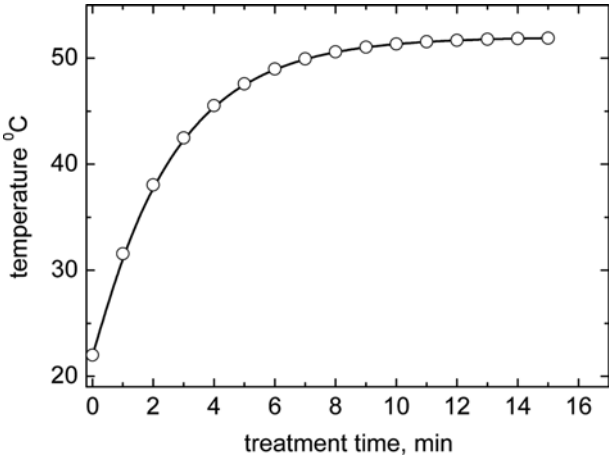

Fig. 8. The change of solution temperature during plasma treatment.

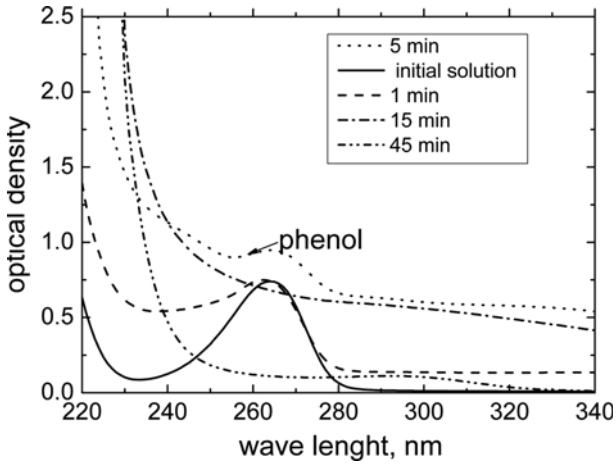

Fig. 9. Change in UV spectrum of solution during plasma treatment. The inset shows the treatment times.

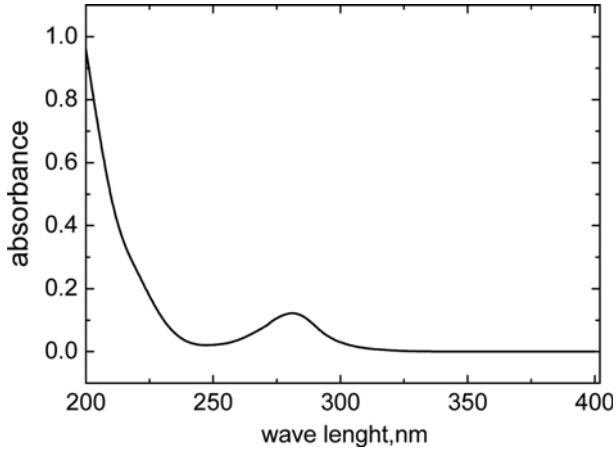

Fig. 10. UV/Vis absorption spectrum of catechol at the concentration of 17 mg/*l*.

The phenol decomposition is accompanied by the formation of intermediate products, which provides the absorption in the range of 240-340 nm and at lower wavelengths than 220 nm. According to Fig. 10, the first compounds are hydroxyphenols and the second are aldehydes, carboxylic acids and hydrogen peroxide. Actually, for hydroxyphenols, absorption disappears during the treatment time (Fig. 6), whereas absorbance in the short-wave range is infinitely increased. The data on concentration changes of carboxylic acids and aldehydes are represented in Fig. 11. As can be seen, these compounds are intermediate ones and changes in their concentrations cannot result in the absorbance increase in the UV region

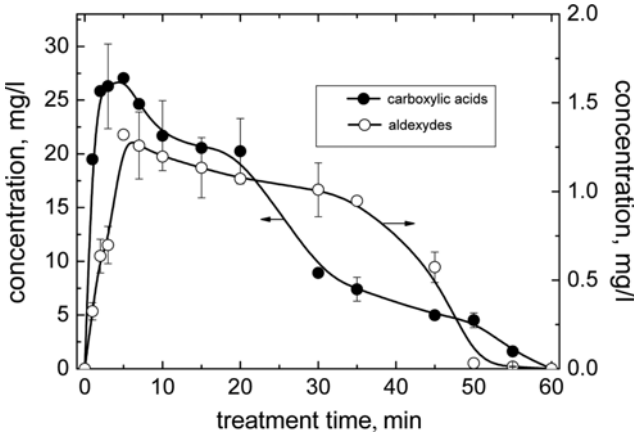

Fig. 11. The total concentration of carboxylic acids and aldehydes as a function of treatment time.

under a significant time of treatment. Probably, this is due to the hydrogen peroxide accumulation. Certainly, HO_2 radicals absorb in the range of 200-240 nm as well. But HO_2 rapidly transforms into H_2O_2 according to $2HO_2 \rightarrow H_2O_2+O_2$ reaction ($K=8\times10^5$ *l*/(mol×s) [5]). Taking into account that the time interval between treatment and measuring is about 15 min, one can register the H_2O_2 absorbance as a product of HO_2 disproportionation.

When comparing the absorption spectrum (Fig. 9) with the optical emission spectrum (Fig. 3), it can be concluded that the plasma radiation must stimulate both phenol decomposition and decomposition of its destruction products, due to the formation of excited molecules:

$$C_6H_5OH+h\nu \rightarrow C_6H_5OH^*$$

UV radiation has to initiate the decomposition of a hydrogen peroxide as well:

$$H_2O_2+h\nu \rightarrow \bullet OH+\bullet OH$$

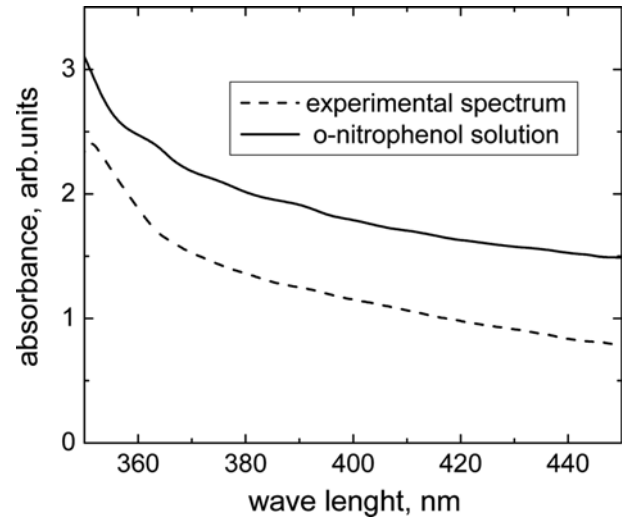

Fig. 12. The comparison of absorption spectra of o-nitrophenol reference solution with the concentration of 0.17 mg/*l* and test solution sampled after 5 min of discharge action.

We assume that the solution with yellow color is determined by the formation of nitro derivatives of phenols. Every absorption spectrum of nitrophenols consists of two bands. Their maximum locations of each band are 350, 340 and 317 nm, and 265, 270 and 278 nm, respectively. Short wavelength range of spectra overlaps with the phenol absorption spectrum (~260 nm, Fig. 9). This is one of the reasons why the phenol concentrations determined by absorption method gave higher values than those obtained with a fluorescent method (Fig. 5). The absorption spectrum of the solution in near-ultraviolet and visible regions is shown in Fig. 12 along with the spectrum of o-nitrophenol for comparison. These spectra are very similar. And the difference can be connected with the real spectrum, which is the superposition of spectra for all three isomers. Extinction coefficients for all nitrophenols are close at a wavelength of 350 nm ($\lg\varepsilon\approx3.1$-3.4 [39]). Therefore, total concentration of nitrophenols can be measured using the o-nitrophenol solution for calibration. The appropriate concentrations obtained in such a manner are shown in Fig. 6.

pH values (Fig. 5) show that a strong acid has to be formed during the discharge treatment. Likewise, chemical analysis discovered the formation of nitrate ions (Fig. 13). Therefore, nitric acid must be formed. And the reaction of this acid with phenol provides the formation of nitrophenols. Nitrogen oxides from a gaseous phase are the sources of nitric acid. The formation of NO is clearly observed in the emission spectrum (Fig. 3).

It can be oxidized to NO_2, HNO_3 and HNO_2:

$$NO+O \rightarrow NO_2, \quad NO+HO_2 \rightarrow HNO_3, \quad NO+H_2O_2 \rightarrow H_2O+NO_2,$$
$$NO_2+OH \rightarrow HNO_3, \quad NO+H_2O_2 \rightarrow OH+HNO_2,$$

The formation of nitrite ions was observed as well (Fig. 14). Since the NO_2^- is thermodynamically unstable in an acid medium, the disproportionation of NO_2^- results in NO and NO_3^-.

Note that nitric acid formation was observed in the other study [40]. Assuming that NO_3^- ions are the products of nitric acid dissociation, we obtain a pH value of ~3 for an NO_3^- concentration of 35 mg/*l*. This value is rather close to an experimental one (Fig. 5), taking into account the existence of other acid compounds in the solution.

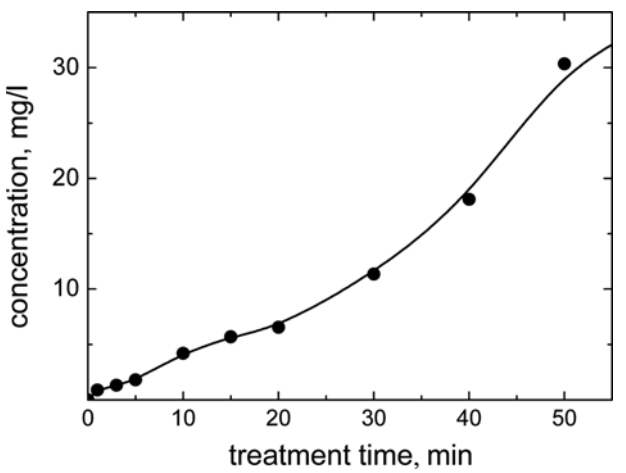

Fig. 13. The concentration of NO_3^- ions as a function of treatment time.

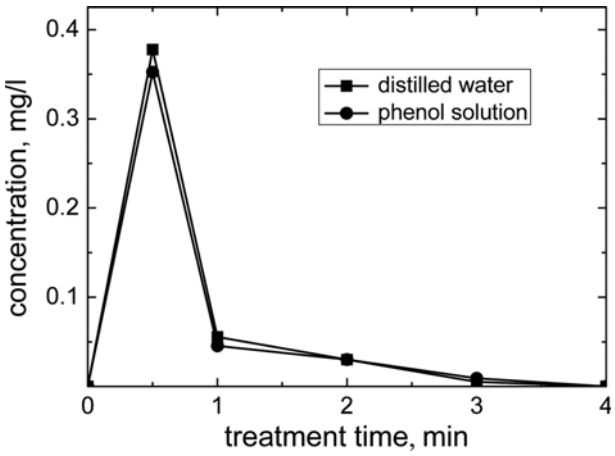

Fig. 14. The concentration of NO_2^- ions as a function of treatment time.

4. Discussion about Probable Mechanism of Phenol Decomposition

The destruction process at oxygen DBD action on phenol hydroxyderivatives was studied in our previous study [41]. It was discovered that carboxylic acids were the main products. In previous studies [42,43] devoted to plasma treatment of acetic and formic acids, it was shown that their decomposition resulted in the formation of appropriate aldehydes and carbon dioxide only, whereas carbon monoxide and dioxide were formed during formaldehyde plasma destruction [44]. Possible reaction pathways of the acids transformation into aldehydes are proposed in previous studies [42,43] as well. In our case, the formation of carboxylic acids and aldehydes was observed as well (Fig. 11). Therefore, it can be assumed that the discharge action stimulates the following chain of oxidative transformations:

phenol→oxyphenols→carboxylic acids
→aldehydes→carbon monoxide and dioxide

To discover a nitrophenol transformation pathway, it is necessary to carry out the special studies.

Table 1 shows the calculation results of carbon balance in the solution at different periods of discharge treatment. In an initial period of discharge action, the balance is close to 100%. But there is a rising discrepancy with increasing the treatment time. We assume that, as mentioned above, it can be due to the formation of gaseous carbon oxides.

Table 1. The yield of decomposition products in percent from initial carbon content in solution

Product	Treatment time, min		
	2	5	10
Phenol (residue)	5.7	1.9	1.6
Oxyphenols	35.6	20.8	13.8
Nitrophenols	13	13	17.1
Carboxylic acids*	26.8	28.1	22.9
Aldexydes**	0.65	1.4	1.2
Total	81.8	65.2	56.6

* - in terms of acetic acid

**- in terms of formaldehyde

CONCLUSION

This study reports the process of DC discharge treatment in ambient air of a phenol solution and the decomposition of solutes. The application of this discharge type was quite efficient. The formation kinetics of the decomposition products was studied as well. Unlike oxygen discharges, air discharge can generate not only oxygen-containing compounds (hydroxyphenols, carboxylic acids, aldehydes) from phenol transformation, but also nitrogen-containing compounds which include nitric and nitrous acids, and products of their interaction with phenol (nitro phenols). Therefore, there are two independent pathways for primary reactions of phenol transformation. The first is the formation of hydroxyphenols and the second is the formation of nitro phenols. During water purification, the formation of nitro phenols and aldehydes is undesirable.

ACKNOWLEDGEMENTS

This study was supported by the Federal Target Program "Scientific and Scientific-Educational Personal of Innovative Russia for 2009-2013," State contract №14.B37.21.0763. This work was also supported by the Korea Research Foundation (KRF-2005-6130) for Local Laboratory Research Project, by the National Research Foundation (NRF) grant funded by the Korea government (MSIP) (NRF-2014R1A2A2A01006994), by the Korea CCS R&D Center (KCRC) grant funded by the Korea government (MSIP) (2014M1A8A1049345).

REFERENCES

1. L. R. Grabowski, E. M. van Veldhuizen, A. J. M. Pemen and W. R. Rutgers, *Plasma Chem. Plasma Process.*, **26**, 3 (2006).
2. J. Gao, Y. Liu, W. Yang, L. Pu, J. Yu and Q. Lu, *Plasma Sources Sci. Technol.*, **12**, 533 (2003).
3. S. Tomizawa and M. Tezuka, *Plasma Chem. Plasma Process*, **27**, 486 (2007).
4. P. Lukes and B. R. Locke, *J. Phys. D: Appl. Phys.*, **38**, 4074 (2005).
5. D. R. Grymonpre, A. K. Sharma, W. C. A. Finney and B. R. Locke, *Chem. Eng. J.*, **82**, 189 (2001).
6. E. S. Bobkova, V. I. Grinevich, N. A. Ivantsova and V. V. Rybkin, *Plasma Chem. Plasma Process.*, **32**, 97 (2012).
7. G.-Z. Qu, N. Lu, J. Li, Y. Wu, G.-F. Li and D. Li, *J. Hazard. Mater.*, **172**, 472 (2009).
8. E. Njoyin, P. Ghogomu, S. Laminsi, S. Nzali, A. Doubla and J. L. Brisset, *Ind. Eng. Chem. Res.*, **48**, 9773 (2009).
9. I. M. Piskarev, *Technical Physics*, **44**, 53 (1999).
10. J. Janca, S. Kuzmin, A. Maximov and J. Titova, *Plasma Chem. Plasma Process.*, **19**, 53 (1999).
11. B. Jiang, J. Zheng, S. Qiu, M. Wu, Q. Zhang, Z. Yan and Q. Xue, *Chem. Eng. J.*, **236**, 348 (2014).
12. E. Tatarova, N. Bundaleska, J. P. Sarette and C. M. Ferreira, *Plasma*

Sources Sci. Technol., **23**, 063002 (2014).
13. E. S. Bobkova, E. S. Ivanova, R. A. Nevedomyi and A. V. Sungurova, *High Energy Chemistry*, **48**, 346 (2014).
14. E. S. Bobkova, D. S. Krasnov, A. V. Sungurova, A. I. Shishkina and T. G. Shikova, *High Energy Chemistry*, **47**, 53 (2013).
15. J. H. Yan, C. M. Du, X. D. Li, B. G. Cheron, M. J. Ni and K. F. Cen, *Plasma Chem. Plasma Process.*, **26**, 31 (2006).
16. G. Eisenberg, *Ind. Eng. Chem. Anal. Ed.*, **15**, 327 (1943).
17. T. Verreycken, D. C. Schram, C. Leys and P. Bruggeman, *Plasma Sources Sci. Technol.*, **19**, 045004 (2010).
18. G. Herzberg, *Molecular Spectra and Molecular Structure: Spectra of Diatomic Molecules*, van Nostrand Co., Princeton (1950).
19. V. A. Titov, V. V. Rybkin, S. A. Smirnov, A. N. Kulentsan and H.-S. Choi, *Plasma Chem. Plasma Process.*, **26**, 543 (2006).
20. J.-L. Brisset, D. Moussa, A. Doubla, E. Hnautic, B. Hnautic, G. K. Joubi, J.-M. Herry, M. Naitali and M.-N. Bellon-Fontaine, *Ind. Eng. Chem. Res.*, **47**, 5761 (2008).
21. S. Ognier, D. Iya-sou, C. Fourmond and S. Cavadias, *Plasma Chem. Plasma Process.*, **29**, 261 (2009).
22. M. A. Malik, *Plasma Sources Sci. Technol.*, **12**, 26 (2003).
23. P. S. Sunka, V. Babicky, M. Clupek, P. Lukes, M. S. Simek, J. Schmidt and M. C. Cernak, *Plasma Sources Sci. Technol.*, **8**, 258 (1999).
24. A. de Luis, J. I. Lombrana, F. Varona and A. Menendez, *Korean J. Chem. Eng.*, **26**, 48 (2009).
25. E. S. Bobkova, T. G. Shikova and V. V. Rybkin, *High Energy Chemistry*, **46**, 141 (2012).
26. B. R. Locke and K.-Y. Shih, *Plasma Sources Sci. Technol.*, **20**, 034006 (2011).
27. L. A. Kuz'micheva, Yu. V. Titova and A. I. Maksimov, *Surf. Eng. Appl. Electrochem.*, **44**, 281 (2008).
28. Y. Matsui, N. Takeushi, K. Sasaki, R. Hayashi and K. Yasuoka, *Plasma Sources Sci. Technol.*, **20**, 034015 (2011).
29. L. Li, A. Nikiforov, Q. Xiong, X. Lu, L. Taghizadeh and C. Leys, *J. Phys. D: Appl. Phys.*, **45**, 125201 (2012).
30. B. Klotz, I. Barnes, K. H. Becker and B. T. Golding, *J. Chem. Soc. Faraday Trans.*, **93**, 1507 (1997).
31. S. Teton, A. Mellouki, G. LeBras and H. Sidebottom, *Int. J. Chem. Kinet.*, **28**, 291 (1996).
32. E. S. Bobkova, S. A. Smirnov, Y. V. Zalipaeva and V. V. Rybkin, *Plasma Chem. Plasma Process.*, **34**, 721 (2014).
33. E. S. Bobkova, T. G. Shikova, V. I. Grinevich and V. V. Rybkin, *High Energy Chemistry*, **46**, 56 (2012).
34. J. Staehelin and J. Hoignt, *Environ. Sci. Technol.*, **16**, 676 (1982).
35. H. Taube and W. C. Bray, *J. Am. Chem. Soc.*, **62**, 3357 (1940).
36. R. E. Buhler, J. Staehelin and J. Hoigne, *J. Phys. Chem.*, **88**, 2560 (1984).
37. J.-L. Brisset and E. Hnatiuc, *Plasma Chem. Plasma Process.*, **32**, 655 (2012).
38. M. Semadeni, D. W. Stocker and J. A. Kerr, *Int. J. Chem. Kinet.*, **27**, 287 (1995).
39. P. J. Linstrom and W. G. Mallard, *NIST Chemistry WebBook*; NIST Standard Reference Database Number 69; National Institute of Standards and Technology: Gaithersburg MD, 2015; http:// webbook.nist.gov, 20899.
40. C. M. Du, Y. W. Sun and X. F. Zhuang, *Plasma Chem. Plasma Process.*, **28**, 523 (2008).
41. A. G. Bubnov, E. Yu. Burova, V. I. Grinevich, V. V. Rybkin, J.-K. Kim and H.-S. Choi, *Plasma Chem. Plasma Process.*, **27**, 177 (2007).
42. E. S. Bobkova, A. A. Isakina, V. I. Grinevich and V. V. Rybkin, *Russian Journ. Appl. Chem.*, **85**, 75 (2012).
43. V. I. Grinevich, N. A. Plastinina, V. V. Rybkin and A. G. Bubnov, *High Energy Chemistry*, **43**, 138 (2009).
44. E. S. Bobkova, V. I. Grinevich, E. Yu. Kvitkova and V. V. Rybkin, *Izv. Vyssh. Uchebn. Zaved., Khim. Khim. Tekhnol.*, **54**, 55 (2011).